Journal of Magnetic Resonance 208 (2011) 44–48

Contents lists available at ScienceDirect

Journal of Magnetic Resonance

journal homepage: www.elsevier.com/locate/jmr

Very fast magic angle spinning ^{1}H-^{14}N 2D solid-state NMR: Sub-micro-liter sample data collection in a few minutes

Yusuke Nishiyama [a,*], Yuki Endo [a], Takahiro Nemoto [a], Hiroaki Utsumi [a], Kazuo Yamauchi [b,1], Katsuya Hioka [a], Tetsuo Asakura [b]

[a] JEOL Ltd., 3-1-2 Musashino, Akishima, Tokyo 196-8558, Japan
[b] Department of Biotechnology, Tokyo University of Agriculture and Technology, Tokyo 184-8588, Japan

ARTICLE INFO

Article history:
Received 9 September 2010
Revised 30 September 2010
Available online 8 October 2010

Keywords:
Solid-state NMR
^{14}N
Very fast MAS
HMQC
1 mm MAS
Micro-coil

ABSTRACT

Substantial resolution and sensitivity enhancements of solid-state ^{1}H detected ^{14}N HMQC NMR spectra at very fast MAS rates up to 80 kHz, in a 1 mm MAS rotor, are presented. Very fast MAS enhances the ^{1}H transverse relaxation time and efficiently decouples the ^{1}H-^{14}N interactions, both effects leading to resolution enhancement. The micro-coil contributes to the sensitivity increase *via* strong ^{14}N rf fields and high sensitivity per unit volume. ^{1}H-^{14}N HMQC 2D spectra of glycine and glycyl-L-alanine at 70 kHz MAS at 11.7 T are observed in a few minutes with a sample volume of 0.8 μL.

1. Introduction

Nitrogen-14. is rarely observed by NMR despite its high natural abundance (99.63%) and its importance in bio and material sciences. The difficulties in observing ^{14}N resonances are due to its integer spin quantum number ($I = 1$) and the related quadrupolar interactions. In solution NMR, quadrupolar relaxation broadens the lineshape leading to non-informative spectra with low resolution. In solid-state NMR, the linewidth is typically a few Megahertz due to the lack of single-quantum (SQ) transitions which are not affected by first order quadrupolar broadening. Together these limitations make ^{14}N spectra difficult to observe.

To solve these problems, both Bodenhausen's group and Gan independently proposed an indirect ^{14}N detection method *via* spin-1/2 nuclei in solid-state with magic-angle-spinning (MAS) NMR [1–4]. The experiments are similar to the heteronuclear multiple quantum coherence (HMQC) experiments used for solution NMR [5], but the magnetization transfer is driven by a combination of *J* coupling [6] and residual dipolar splittings (RDS) with rotor synchronous observation in the indirect dimension. This method is referred to as *J*-HMQC. For the initial reports, ^{13}C was used as the spin-1/2 nucleus [1,2]. This ensures good signal separation by virtue of the high resolution in the ^{13}C direct detection dimension, although ^{13}C isotopic enrichment was required. ^{1}H observation has also been utilized to enhance sensitivity [7]. Magic angle spinning, in *J*-HMQC experiments, removes first order broadening of the ^{14}N SQ transitions leading to extensive spinning sideband manifolds. The spinning sideband manifolds are folded into the same ^{14}N position by setting the t_1 increment to $1/\nu_r$, where ν_r is the spinning frequency. Stable sample spinning is required to maintain optimal folding of the spinning sidebands. Precise magic angle setting is required to avoid reintroducing the first order broadening. The resulting lineshape and position in the SQ spectra are free from first order quadrupolar broadening and are then dominated by second- and third-order quadrupolar terms and some cross terms [4]. The double quantum (DQ)-HMQC experiments avoid the requirement of stable sample spinning, precise magic angle setting, and additional third-order broadening. Indeed, since the DQ transition is a symmetric transition, DQ coherence does not include first- and third-order quadrupolar broadening. However, DQ-HMQC suffers from low sensitivity due to poor excitation efficiency.

Several improvements have been proposed for ^{1}H-^{14}N HMQC experiments. First, sensitivity can be enhanced by utilizing heteronuclear dipolar interactions instead of the combination of *J* and RDS for magnetization transfer, leading to the *D*-HMQC experiment [8–11]. The sensitivity enhancement was achieved by applying ^{1}H rf field in magnetization transfer periods to recouple the ^{1}H-^{14}N heteronuclear dipolar interaction and decouple ^{1}H-^{1}H interactions.

* Corresponding author. Address: NM Business unit, JEOL Ltd., 3-1-2 Musashino, Akishima, Tokyo 196-8558, Japan. Fax: +81 42 546 8068.
E-mail address: yunishiy@jeol.co.jp (Y. Nishiyama).
[1] Present address: King Abdullah University of Science and Technology, Thuwal, Saudi Arabia.

1090-7807/$ - see front matter © 2010 Elsevier Inc. All rights reserved.
doi:10.1016/j.jmr.2010.10.001

The much larger ^{1}H-^{14}N dipolar coupling, relative to *J* or RDS, enhances the magnetization transfer resulting in a reduction of both the excitation and reconversion periods. This minimizes the transverse relaxation (T_2') decay and hence improves the overall sensitivity. Internuclear distances between spin-1/2 nuclei and ^{14}N have even been reported from the build-up curve of the dipolar transfer [12,13]. Second, resolution enhancement in the ^{14}N dimension was achieved by storing the magnetization along the magnetic field during the t_1 period [14,15]. This reduces the broadening from T_2' decay; however, the sensitivity is halved by incomplete magnetization storage. Third, partial deuteration [7,10,14,15] or ^{1}H-^{1}H homonuclear dipolar decoupling during the t_1 period have been used to enhance ^{14}N resolution by increased ^{1}H T_2' [16]. Fourth, sensitivity enhancement by combining ^{13}C-^{14}N *D*-HMQC and dynamic nuclear polarization was recently reported [17]. Detecting dynamics on 100 ns time scale [18] has also been achieved using the molecular motion sensitive SQ coherences in the ^{1}H-^{14}N HMQC experiment. ^{1}H-^{14}N *D*-HMQC filtering methods for spectral editing [19,20], and three dimensional correlation among ^{1}H, ^{13}C, and ^{14}N [11] have also been reported.

We show here that very fast MAS enhances both sensitivity and resolution in ^{1}H-^{14}N HMQC experiments. The results were obtained with a recently developed 1 mm very fast MAS rotor system [21]. This results in ^{1}H-^{14}N HMQC experimental times of several minutes, even for the volume limited sample of 0.8 μL at 11.7 T.

2. ^{1}H-^{14}N HMQC with very fast MAS

Very fast MAS with a small rotor diameter has several advantages for ^{1}H-^{14}N HMQC experiments on limited volume samples: (1) Enhanced ^{1}H T_2' relaxation times. This leads to resolution and sensitivity enhancements not only in the ^{1}H dimension but also in the ^{14}N dimension by reducing ^{1}H T_2' decay during t_1 and t_2. Very fast MAS also reduces ^{1}H T_2' decay during the excitation and reconversion periods in the *J*-HMQC experiment. (2) Wide spectral width for the ^{14}N dimension with rotor-synchronization of the t_1 increment, $\Delta t_1 = 1/\nu_r$. This allows the wide spectral widths required for the ^{14}N dimension due to the large second order quadrupolar shift. (3) Efficient ^{1}H-^{14}N heteronuclear decoupling, which the simple ^{1}H π pulse in the middle of the ^{14}N t_1 evolution period cannot completely accomplish. (4) High sensitivity per unit volume. (5) Strong ^{14}N rf field, leading to efficient excitation of the ^{14}N nuclei. Features 1–3 are the result of using very fast MAS and 4, 5 are from the micro-coil design.

3. Pulse sequence

The pulse sequences for *J*-HMQC (a) and *D*-HMQC (b) are shown in Fig. 1, both are phase cycled to select the SQ coherence pathways unless otherwise specified. The interval between the centers of the two ^{14}N pulses should be synchronized with sample spinning, i.e. $t_1 = n\tau_r$, where n is an integer and $\tau_r = 1/\nu_r$. HMQC filtered 1D ^{1}H spectra, which show ^{1}H signals correlated to ^{14}N sites, were obtained at $t_1 = n_0\tau_r$, where n_0 is the minimum integer to prevent overlap of the two ^{14}N pulses. The value of n_0 is one in most cases, but could be larger for long ^{14}N pulse widths. In the *J*-HMCQ experiment, no ^{1}H rf field was applied during the magnetization transfer periods, and the transfer was driven by a combination of *J*-coupling and RDS. The ^{14}N pulse length and magnetization transfer periods of $t_{exc} = t_{rec}$ were experimentally optimized to maximize the magnetization observed in the *J*-HMQC filtered 1D ^{1}H spectra for each experiment. In the *D*-HMQC experiment the $SR4_1^2$ pulse sequence was applied during the excitation and reconversion periods to decouple the ^{1}H homonuclear dipolar interactions and recouple the ^{1}H-^{14}N heteronuclear dipolar interactions [22]. The $SR4_1^2$ is a supercycled sequence which consists of three pairs of symmetry based sequences, $R4_1^2R4_1^{-2}$. Indeed, $SR4_1^2$ can be written as $[R4_1^2R4_1^{-2}]_0\,[R4_1^2R4_1^{-2}]_{120}\,[R4_1^2R4_1^{-2}]_{240}$. Although the full cycle time of the $SR4_1^2$ sequence lasts six rotor cycles, the length of excitation and reconversion periods were carefully adjusted to even multiples of the rotor period with the $[R4_1^2\,R4_1^{-2}]_\varphi$ sub-unit. *D*-HMQC filtered 1D ^{1}H spectra were used to experimentally optimize the ^{14}N pulse width, the length of $SR4_1^2$ period, and the $SR4_1^2$ rf field strength. The single pulse ^{1}H NMR spectra were obtained with DEPTH background-signal suppression [23].

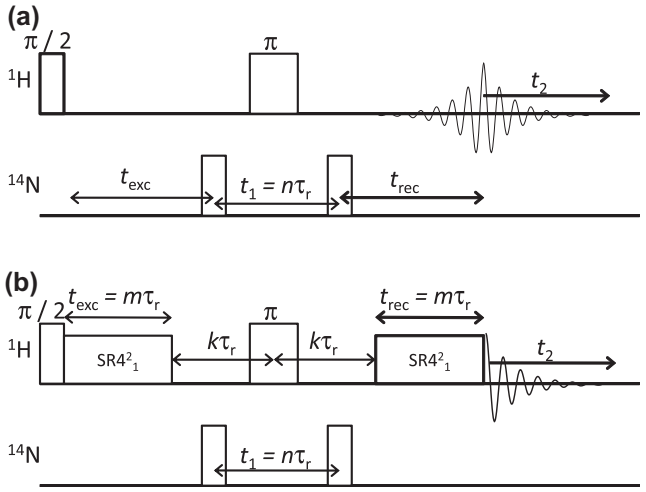

Fig. 1. ^{1}H-^{14}N correlation pulse sequence for *J*-HMQC (a) and *D*-HMQC (b). ^{14}N SQ coherences are selected by phase cycling of ^{14}N pulses in the both sequences. In *D*-HMQC experiment, $SR4_1^2$ spanning $m\tau_r$ is applied during excitation and reconversion periods. Interval between $SR4_1^2$ sequence and π pulse, $k\tau_r$, must be precisely synchronized with the rotor period to maximize echo. The evolution time t_1 must also be rotor-synchronized.

4. Results and discussion

The ^{1}H T_2' values, with and without $SR4_1^2$ irradiation, were obtained by omitting the ^{14}N pulses in the *J*-HMQC and *D*-HMQC sequences, respectively, with appropriate phase cycling. Glycine ^{1}H T_2' relaxation measurements at various spinning frequencies are presented in Fig. 2. The ^{1}H T_2' relaxation time without ^{1}H irradiation increases linearly with increasing spinning frequency;

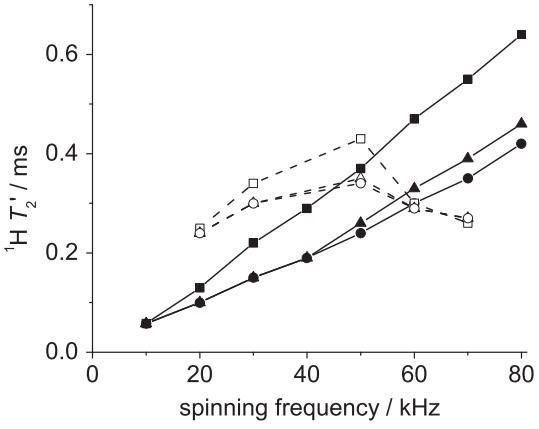

Fig. 2. Transverse relaxation time of ^{1}H nuclei in glycine with $SR4_1^2$ irradiation (□△○) and without $SR4_1^2$ irradiation (■▲●) at various spinning frequencies. NH_3^+ protons (□■) and the two inequivalent CH_2 protons (△○▲●) are shown.

however, the ^{1}H T_2' relaxation time with $SR4_1^2$ ^{1}H irradiation shows little spinning frequency dependence.

Fig. 3a shows single pulse ^{1}H NMR spectra at various spinning frequencies. The signal intensity increases with the spinning frequency. This shows that the ^{1}H linewidth is mainly dominated by ^{1}H T_2'. The *J*-HMQC filtered ^{1}H NMR spectra also show large sensitivity enhancements as a function of spinning speed (Fig. 3b). Only the NH_3^+ signal is observed, because the magnetization transfer is primarily driven by the through-bond *J* coupling. The experimentally optimized t_{exc} increases as spinning frequency increases. This shows that the ^{1}H T_2' dominates the build-up curve for the magnetization transfer between ^{1}H and ^{14}N in *J*-HMQC experiments. Despite the sensitivity enhancement with very fast MAS, the resultant *J*-HMQC filtered ^{1}H signal intensity at 80 kHz is only 0.44% of the ^{1}H single pulse MAS NMR spectrum. Further sensitivity enhancement is achieved with heteronuclear dipolar recoupling during magnetization transfer (Fig. 3c). The *D*-HMQC filtered ^{1}H NMR spectrum shows a 19-fold sensitivity enhancement at 70 kHz over the *J*-HMQC filtered ^{1}H NMR spectrum. The reduction of t_{exc} and improved magnetization transfer result in the larger signal enhancement. The experimentally optimized t_{exc} of ca 300 μs for the *D*-HMQC filtered spectra is little dependent on spinning frequency relative to the increasing t_{exc} value for the *J*-HMQC filtered spectra. This is expected because the ^{1}H T_2' relaxation times with $SR4_1^2$ recoupling are nearly independent on spinning frequency and the recoupled dipolar interaction is theoretically independent on spinning frequency in the first order average Hamiltonian. The sensitivity enhancement with increasing spinning frequency in the *D*-HMQC filtered ^{1}H spectra is due: (i) to enhancement of signal intensity in the t_2 dimension, (ii) to the reduction of T_2' decay during t_1, and (iii) to the reduction of minimum $t_1 = n_0\tau_r = n_0/\nu_r$. These effects can be calculated with the following equation for the expected signal intensity of *D*-HMQC filtered spectra $I_{calc}(\nu_r)$:

$$I_{calc}(\nu_r) \propto I(\nu_r)\exp\left(-\frac{t_1}{T_2'(\nu_r)}\right) = I(\nu_r)\exp\left(-\frac{n_0}{\nu_r T_2'(\nu_r)}\right), \quad (1)$$

where $I(\nu_r)$ is signal intensity of ^{1}H single pulse spectra and $T_2'(\nu_r)$ is the T_2' value at ν_r MAS. The calculated intensity curve is overlaid on Fig. 3c, with $n_0 = 1$ for all spinning frequencies. This equation assumes a constant ^{1}H-^{14}N-^{1}H transfer efficiency, and thus constant ^{14}N rf-pulses. The calculated results agree well with the observed signal intensities. Note that in addition to the NH_3^+ signal, a CH_2 signal is also present in Fig. 3c, because the magnetization transfer is through-space *via* the ^{1}H-^{14}N dipolar interaction. The longer ^{1}H-^{14}N internuclear distance between the ^{14}N-(C)H_2 site versus the ^{14}N-(N)H_3 site leads to the weaker ^{14}N-(C)H_2 signal. The internuclear distance can be estimated by observing the ^{1}H-^{14}N build-up curve [13].

The ^{1}H signal intensity for *D*-HMQC filtered ^{1}H spectrum ($I_{D\text{-edit}}$) at 70 kHz MAS is 7% of the single pulse excitation (I_{sp}). This is much stronger than the 0.44% found when comparing the *J*-HMQC filtered ^{1}H spectrum ($I_{J\text{-edit}}$) at 80 kHz MAS to I_{sp}. The 70 kHz MAS ^{1}H spin echo magnetization (I_{echo}) with $SR4_1^2$ irradiation at $t_1 = \tau_r$ is 47% of I_{sp} and the comparison $I_{D\text{-edit}}$ to I_{echo} is 15%. This shows that the low transfer efficiency of magnetization from ^{1}H to ^{14}N and back to ^{1}H limits the sensitivity of the *D*-HMQC experiment. The main origin of poor efficiency thus comes from the limited ^{14}N rf field strength.

Fig. 4 illustrates the dependence of signal intensity on ^{14}N rf field strength at 70 kHz MAS. The glycine sample, with a relatively small quadrupolar coupling of qcc ~ 1 MHz, shows little dependence on

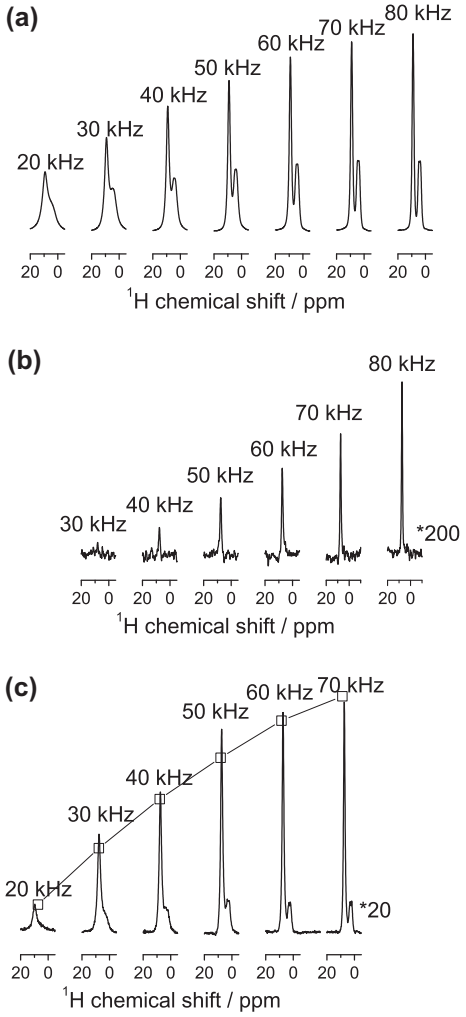

Fig. 3. Single pulse (a), *J*-HMQC filtered (b), and *D*-HMQC filtered (c) ^{1}H spectra of glycine at various spinning frequencies. *J*-HMQC and *D*-HMQC filtered spectra were displayed with 200 and 20 times magnification. DEPTH background suppression was applied to the ^{1}H single pulse spectra to remove signals from outside the sample coil [23]. HMQC filtered ^{1}H spectra were obtained after optimizing the experimental conditions, i.e. the length of excitation and reconversion periods and the ^{14}N pulse lengths and amplitudes, to maximize the signal strength at each spinning frequency. The optimized t_{exc} in (b) and (c) are N.A. and 200 μs for 20 kHz, 200 μs and 267 μs for 30 kHz, 200 μs and 250 μs for 40 kHz, 300 μs and 280 μs for 50 kHz, 500 μs and 267 μs for 60 kHz, 600 μs and 286 μs for 70 kHz, and 700 μs and N.A. for 80 kHz, respectively. The curve calculated from Eq. (1) is overlaid on (c).

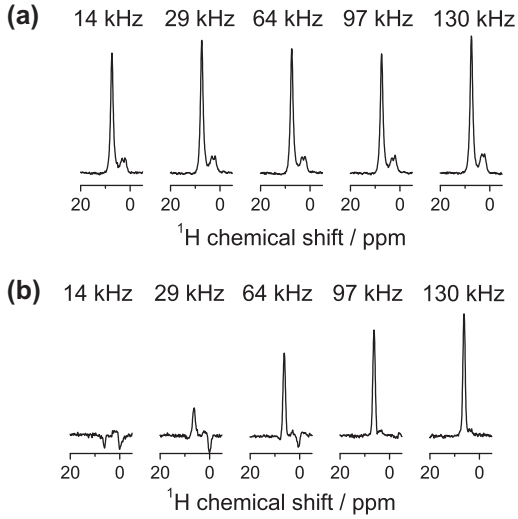

Fig. 4. *D*-HMQC filtered ^{1}H spectra of (a) glycine and (b) L-alanyl-L-alanyl-L-alanine at various ^{14}N rf field strengths of 14 kHz, 29 kHz, 64 kHz, 97 kHz, and 130 kHz from left to right. All the spectra were observed at 70 kHz MAS.

the ^{14}N rf field strength. On the other hand, signal intensities are greatly enhanced by strong ^{14}N rf irradiation strength for L-alanyl-L-alanyl-L-alanine, with the larger quadrupolar coupling for the peptide nitrogens, typically 3–4 MHz. The increasing signal as a function of increasing ^{14}N rf field strength clearly shows the advantage of the larger ^{14}N rf fields obtained with the small rotor diameter and micro-coil.

The 2D correlation ^{1}H-^{14}N *D*-HMQC spectrum of glycine at 70 kHz is presented in Fig. 5. The experimental time was 3 min with 128 t_1 points, 2 scans per t_1 point, and a relaxation delay of 0.35 s. This is the smallest number of scans required to select the ^{14}N SQ coherences. Pulsed field gradients would allow further reduction in the number of scans [24]. Even with the volume limited sample of only 0.8 μL the ^{1}H-^{14}N correlations have good signal to noise ratio. The correlations are visible not only between nitrogen and protons in NH_3^+ moiety, which are directly bonded, but also between NH_3^+ nitrogen and CH_2 protons, which are separated by two bonds. The spectral width of 70 kHz is sufficient for most ^{14}N samples.

Fig. 6 shows the slices along the ^{14}N dimension from ^{1}H-^{14}N *D*-HMQC spectra of glycine at spinning frequencies of 20 kHz and 70 kHz, and a calculated ^{14}N spectrum using the previously reported quadrupolar coupling parameters of qcc = 1.25 MHz, and $\eta = 0.51$ [25]. The calculated spectrum, up to the second-order, agrees well with the experimental slice at 70 kHz. This indicates that the ^{1}H-^{14}N heteronuclear dipolar interactions are well decoupled and have little effect on linewidth at very fast MAS rates; the ^{14}N lineshape is thus mainly dominated by second- and higher-order quadrupolar broadening. On the other hand, the lineshape at 20 kHz MAS is broadened to 1.8 kHz which is 2.3 times broader than the linewidth at 70 kHz. This broadening is caused by inefficient dipolar decoupling of ^{1}H and ^{14}N, and short ^{1}H T_2' during the t_1 period at the slower MAS speed.

Fig. 7 shows a ^{1}H-^{14}N *D*-HMQC spectrum of glycyl-L-alanine at 70 kHz MAS. The experimental time was 2 min with 16 t_1 points, 2 scans per t_1 point, and a relaxation delay of 2 s. There are two chemically inequivalent nitrogen sites in the molecule: the NH_3^+ with a smaller quadrupolar coupling and the NH with a larger

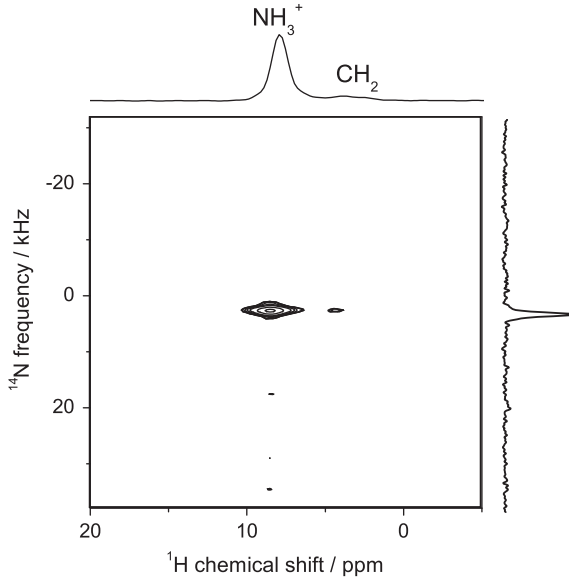

Fig. 5. ^{1}H-^{14}N *D*-HMQC spectrum of glycine at 70 kHz MAS at 11.7 T. Single quantum coherences were selected in the ^{14}N dimension. An $SR4_1^2$ recoupling period of 18 τ_r (257 μs) was applied during both the excitation and reconversion periods. 128 rotor-synchronized t_1 increments ($\Delta t_1 = 1/\nu_r = 14.3$ μs) with 2 scans per t_1 point were collected. The total number of scans was 512. The ^{14}N pulse widths were 11.5 μs, applied at 2.9 kHz (81 ppm). Slices along ^{1}H and ^{14}N dimensions are also shown.

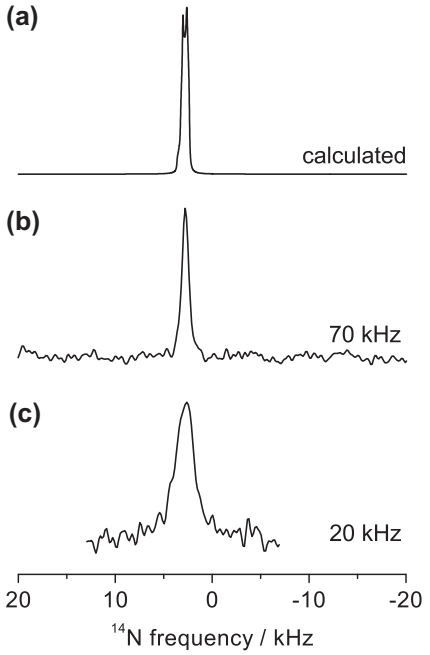

Fig. 6. Calculated ^{14}N spectrum and ^{14}N slices of experimental ^{1}H-^{14}N *D*-HMQC spectra of glycine: calculated (a), experimental at 70 kHz (b), and experimental at 20 kHz (c). Spectrum (a) was calculated using the previously reported values (qcc = 1.25 MHz and $\eta = 0.51$) [25].

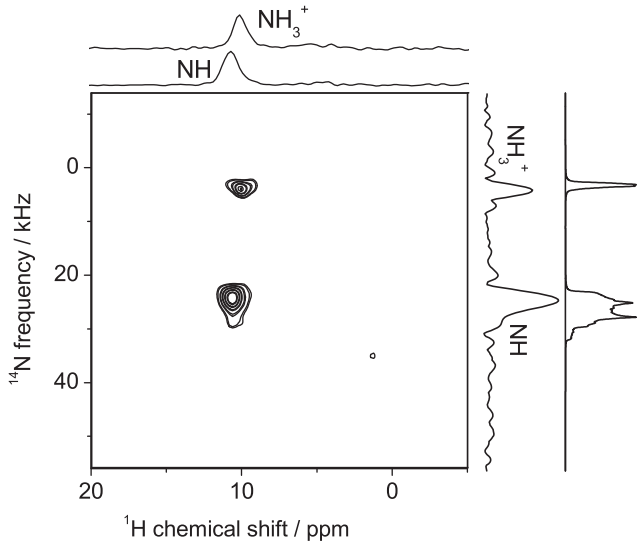

Fig. 7. ^{1}H-^{14}N *D*-HMQC spectrum of glycyl-L-alanine at 70 kHz MAS at the magnetic field of 11.7 T. Single quantum coherences were selected in the ^{14}N dimension. An $SR4_1^2$ recoupling period of 8 τ_r (114 μs) was applied during both the excitation and reconversion periods. 16 rotor-synchronized t_1 increments ($\Delta t_1 = 1/\nu_r = 14.3$ μs) with 2 scans per t_1 point were collected. Total number of scans was 64. The ^{14}N pulse widths were 7 μs and applied at 21.0 kHz (581 ppm). ^{1}H slices through the two ^{1}H-^{14}N resonances, and experimental and calculated ^{14}N projections are also shown. Calculated spectra were obtained using the previously reported values (qcc = 3.25 MHz, $\eta = 0.4$ for NH and qcc = 1.25 MHz, $\eta = 0.51$ for NH_3^+) [25].

quadrupolar coupling. The peak positions in the ^{14}N dimension are dominated by second order isotropic quadrupolar shift resulting in a peak separation of almost 30 kHz. Very fast MAS with wide spectral widths prevent signal folding in the ^{14}N dimension. Calculated spectra with qcc = 3.25 MHz, $\eta = 0.4$ for the NH [25], and qcc = 1.25 MHz, $\eta = 0.51$ for the NH_3 (the same values as NH_3 of glycine), are also shown in Fig. 7. The calculated spectra agree well with the experimental spectra. The signals are also slightly

separated in the ^{1}H dimension as shown by the peak separation for the ^{1}H slices through the two cross peaks.

We found that ^{1}H-^{14}N *D*-HMQC spectra can contain strong t_1-noise ridges near the maximum MAS frequency of 80 kHz, although no t_1-noise is observed in ^{1}H-^{14}N *J*-HMQC spectra. Some t_1-noise at 70 kHz is visible in the ^{14}N slices and projections (Figs. 5 and 7, respectively). The t_1-noise in *D*-HMQC is caused by short-term fluctuations of the sample spinning at 80 kHz, not by spectrometer instabilities as found in standard solution NMR spectra. Since the recoupled dipolar interaction depends on rotor phase, the excitation and reconversion, $SR4_1^2$ timing must be carefully synchronized with MAS speed; even a small rotor phase difference between excitation and reconversion leads incomplete echo formation, resulting in t_1-noise. This was supported by the absence of t_1-noise in ^{1}H-^{14}N *J*-HMQC even at 80 kHz, because the *J* and RDS interactions have a small dependence on rotor phase. The t_1-noise hampers the observation of 2D *D*-HMQC and *D*-HMQC filtered 1D ^{1}H NMR at 80 kHz. Active synchronization of excitation and reconversion sequence to sample spinning should reduce the t_1-noise [13,26]. Alternatively, this problem could be solved by continuously notifying the instantaneous spinning frequency and updating the pulse sequence timing. This results in the correct timing for the pulse sequence even if the spinning speed is fluctuating from scan to scan.

5. Conclusion

The sensitivity and resolution enhancement found in ^{1}H-^{14}N HMQC experiments with very fast MAS were examined. *D*-HMQC filtering offers 19-fold sensitivity enhancement over *J*-HMQC filtering. Very fast MAS improves both sensitivity and resolution not only the ^{1}H dimension but also in ^{14}N dimension *via* the reduction of ^{1}H T_2' decay and efficient ^{1}H-^{14}N heteronuclear dipolar decoupling. The strong ^{14}N rf field greatly enhances the HMQC filtering especially for systems with larger quadrupolar coupling constants. Compared to the single pulse ^{1}H intensity for glycine, the 7% ^{1}H *D*-HMQC filtered signal intensity is sufficient to allow the collection of ^{1}H-^{14}N 2D HMQC spectra with good signal-to-noise in a few minutes even for the limited 0.8 μL sample volume.

6. Experimental

6.1. Materials

Glycine, glycyl-L-alanine, and L-alanyl-L-alanyl-L-alanine were purchased from Tokyo Chemical Industry Ltd., Sigma–Aldrich Co., and Bachem AG (Bubendorf, Switzerland), respectively. All samples were used without isotopic labeling. The volume for each sample was 0.8 μL.

6.2. NMR experiments

The solid-state NMR experiments were performed at ^{1}H frequencies of 500 MHz (11.7 T) using a JEOL JNM-ECA system equipped with a JEOL 1.0 mm CPMAS probe. Experimental ^{14}N shifts were externally referenced to NH_4Cl at 0 Hz. All data were collected at ambient probe temperatures. The sample spinning speed was actively stabilized with a pneumatic solenoid valve so that the spinning fluctuations were less than ±10 Hz over the 80 kHz spinning speeds accessible to the 1 mm MAS probe. The angle between the spinning axis and the magnetic field was precisely adjusted to minimize the linewidth of ^{1}H-^{14}N *D*-HMQC spectra of glycine in the ^{14}N dimension. ^{1}H-^{14}N *D*-HMQC spectra of glycine are observed before and after the measurement, to ensure the magic angle is maintained during the measurement. The probe was modified to tightly fit to the magnet so that the precise magic angle can be reproduced when the probe is removed and reinserted.

The ^{1}H rf field strength for the excitation $\pi/2$ pulse (1.26 μs) and refocusing π pulse (2.52 μs) was 200 kHz. The ^{14}N rf field strength was 130 kHz unless otherwise noted.

Acknowledgments

The authors would like to thank to M.H. Frey for carefully reading the manuscript. This work was financially supported by JST-SENTAN project.

References

[1] S. Cavadini, A. Lupulescu, S. Antonijevic, G. Bodenhausen, Nitrogen-14 NMR spectroscopy using residual dipolar splittings in solids, J. Am. Chem. Soc. 128 (2006) 7706.
[2] Z. Gan, Measuring amide nitrogen quadrupolar coupling by high-resolution ^{14}N/^{13}C NMR correlation under magic-angle spinning, J. Am. Chem. Soc. 128 (2006) 6040.
[3] S. Cavadini, S. Antonijevic, A. Lupulescu, G. Bodenhausen, Indirect detection of nitrogen-14 in solid-state NMR spectroscopy, Chem. Phys. Chem 8 (2007) 1363–1374.
[4] S. Cavadini, Indirect detection of nitrogen-14 in solid-state NMR spectroscopy, Prog. Nucl. Magn. Reson. Spectrosc. 56 (2010) 46.
[5] L. Müller, Sensitivity enhanced detection of weak nuclei using heteronuclear multiple quantum coherence, J. Am. Chem. Soc. 101 (1979) 4481–4484.
[6] D. Massiot, F. Fayon, B. Alonso, J. Trébosc, J.-P. Amoureux, Chemical bonding differences evidenced from *J*-coupling in solid state NMR experiments involving quadrupolar nuclei, J. Magn. Reson. 164 (2003) 160–164.
[7] S. Cavadini, S. Antonijevic, A. Lupulescu, G. Bodenhausen, Indirect detection of nitrogen-14 in solids via protons by nuclear magnetic resonance spectroscopy, J. Magn. Reson. 182 (2006) 168–172.
[8] Z. Gan, ^{13}C/^{14}N heteronuclear multiple-quantum correlation with rotary resonance and REDOR dipolar recoupling, J. Magn. Reson. 184 (2007) 39–43.
[9] Z. Gan, J.-P. Amoureux, J. Trebosc, Proton-detected ^{14}N MAS NMR using homonuclear decoupled rotary resonance, Chem. Phys. Lett. 435 (2007) 163–169.
[10] S. Cavadini, A. Abraham, G. Bodenhausen, Proton-detected nitrogen-14 NMR by recoupling of heteronuclear dipolar interactions using symmetry-based sequences, Chem. Phys. Lett. 445 (2007) 1–5.
[11] R. Siegel, J. Trebosc, J.-P. Amoureux, Z. Gan, 3D ^{1}H–^{13}C-^{14}N correlation solid-state NMR spectrum, J. Magn. Reson. 193 (2008) 321–325.
[12] Z. Gan, Measuring multiple carbon–nitrogen distances in natural abundant solids using R-RESPDOR NMR, Chem. Commun. (2006) 4712–4714.
[13] L. Chen, Q. Wang, B. Hu, O. Lafon, J. Trebosc, F. Deng, J.-P. Amoureux, Measurement of hetero-nuclear distances using a symmetry-based pulse sequence in solid-state NMR, Phys. Chem. Chem. Phys. 12 (2010) 9395–9405.
[14] S. Cavadini, A. Abraham, G. Bodenhausen, Coherence transfer between spy nuclei and nitrogen-14 in solids, J. Magn. Reson. 190 (2008) 160–164.
[15] S. Antonijevic, N. Halpern-Manners, Probing amide bond nitrogens in solids using ^{14}N NMR spectroscopy, Solid State Nucl. Magn. Reson. 33 (2008) 82–87.
[16] S. Cavadini, V. Vitzthum, S. Ulzega, A. Abraham, G. Bodenhausen, Line-narrowing in proton-detected nitrogen-14 NMR, J. Magn. Reson. 202 (2010) 57–63.
[17] V. Vitzthum, M.A. Caporini, G. Bodenhausen, Solid-state nitrogen-14 nuclear magnetic resonance enhanced by dynamic nuclear polarization using a gyrotron, J. Magn. Reson. (2010) 177–179.
[18] S. Cavadini, A. Abraham, S. Ulzega, G. Bodenhausen, Evidence for dynamics on a 100 ns time scale from single- and double-quantum nitrogen-14 NMR in solid peptides, J. Am. Chem. Soc. 130 (2008) 10850–10851.
[19] J.-P. Amoureux, J. Trebosc, B. Hu, N. Halpern-Manners, S. Antonijevic, High-resolution ^{14}N-edited ^{1}H–^{13}C correlation NMR experiments to study biological solids, J. Magn. Reson. 194 (2008) 317–320.
[20] J.-P. Amoureux, Q. Wang, Bingwen Hu, O. Lafon, J. Trebosc, F. Deng, Rapid analysis of isotopically unmodified amino acids by high-resolution ^{14}N-edited ^{1}H–^{13}C correlation NMR spectroscopy, Chem. Commun. (2008) 6525–6527.
[21] Y. Endo, Y. Nishiyama, K. Yamauchi, K. Hioka, T. Asakura, Very fast magic angle spinning up to 80 kHz 51th ENC abstracts (2010).
[22] A. Brinkmann, A.P.M. Kentgens, Proton-selective ^{17}O–^{1}H distance measurements in fast magic-angle-spinning solid-state NMR spectroscopy for the determination of hydrogen bond lengths, J. Am. Chem. Soc. 128 (2006) 14758–14759.
[23] D.G. Cory, W.M. Ritchey, Suppression of signals from the probe in bloch decay spectra, J. Magn. Reson. 80 (1988) 128–132.
[24] A. Maudsley, Q. Wokaun, R.R. Ernst, Coherence transfer echoes, Chem. Phys. Lett. 55 (1978) 9–14.
[25] D.T. Edmonds, P.A. Speight, Nitrogen quadrupole resonance in amino acids, Phys. Lett. 34A (1971) 325–326.
[26] J. Trebosc, O. Lafon, B. Hu, J.-P. Amoureux, Indirect high-resolution detection for quadrupolar spin-3/2 nuclei in dipolar HMQC solid-state NMR experiments, Chem. Phys. Lett. 496 (2010) 201–207.